Experimental validation of a Pulsating Heat Pipe transient model during the start-up in micro-gravity environment

Mauro Abela, Mauro Mameli, Vadim S Nikolayev, Sauro Filippeschi

Experimental validation of a Pulsating Heat Pipe transient model during the start-up in micro-gravity environment

Mauro Abela[1], Mauro Mameli[1], Vadim Nikolayev[2], Sauro Filippeschi[1]
[1]DESTEC, University of Pisa, Largo L. Lazzarino, Pisa, Italy.
[2]Université Paris-Saclay, CEA, CNRS, SPEC, 91191 Gif-sur-Yvette Cedex, France.

E-mail: mauro.abela@phd.unipi.it

Abstract. A large diameter Pulsating Heat Pipe (PHP) is a device operating as a thermosyphon on ground and as a PHP under microgravity conditions. Such a prototype with a transparent (sapphire) tube section in the adiabatic region has been tested during the 67th ESA parabolic flight campaign. Infrared visualizations of the fluid in the sapphire section along with measurements of all the relevant quantities, which characterize the device state (pressures, temperatures), are acquired during the tests and exploited for the validation of CASCO code of PHP simulation. After accurate implementation of the PHP geometry and material properties, transient simulations have been carried out. A comparison with the experiment is possible only for the cases where the PHP can be initially assumed at equilibrium. The transients for tube wall temperatures, liquid plug velocities, lengths and temperatures show a good agreement with the experiments during the start-up phase in microgravity conditions reducing the gap towards the development of a fully validated PHP design tool.

1. Introduction

The use of PHPs under weightlessness have been discussed since long time [1, 2]. A PHP with a channel of a large diameter (larger than the critical diameter defined for the Earth gravity) can be more advantageous because of small viscous losses. It remains a capillary in the weightlessness so is expected to function as a PHP there. Such a device acts however as a loop thermosyphon on Earth [3]. In this work we test such a device under weightlessness and compare the experimental results to the numerical simulations performed with the CASCO software (French abbreviation for Code Avancé de Simulation de Caloduc Oscillant, advanced PHP Simulation code) [4–6].

2. Experiment

The device designed by the University of Pisa is a closed loop aluminum tube with an inner and outer diameter of 3mm and 5mm, respectively, folded in 14 turns (Fig. 1) and partially filled with 22 ml of FC-72 (50% volumetric filling ratio). An aluminum heat spreader brazed on the tube is heated by two ceramic Joule alumina heaters thus forming the evaporator zone. Two spreaders brazed on the tube are cooled down with a Peltier cell system coupled with a temperature regulation that imposes $T_c = 20°C$ condenser temperature. One tube section is

made of sapphire glass to observe the flow pattern and temperature with the IR camera and high-speed grey-scale camera. At the ends of the sapphire tube, a pressure transducer and two

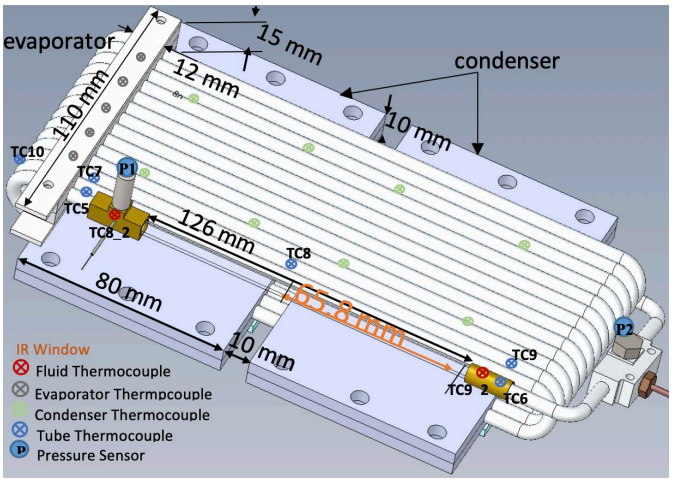

Figure 1. The tube temperature is measured with the thermocouples TC 5-TC10, while the fluid temperature, with the thermocouples TC8_2, TC9_2. The fluid pressure is measured with the pressure transducers P1, P2. Some of thermocouples are located inside the evaporator spreader block, some inside the condenser blocks. The size of the transparent PHP branch is shown together with the position and length of its portion observed with the IR camera (IR window).

K-type micro-thermocouples are installed inside the tube to measure the liquid temperature. Five T-type thermocouples are located between the evaporator spreader and heater; six are located between the Peltier cold side and the condenser spreader; two on top of the condenser spreader; seven are located on the tube external wall. The heating power is provided by a programmable power supply. The parabolic flight campaign lasted three days, during each day thirty-one parabolic maneuvers have been performed: the first parabola was followed by six sequences of five consecutive parabolas; after each sequence a five minutes break of steady flight was taken. Each parabola is a series of hyper-gravity period (20±2 s at 1.8g), micro-gravity period (20±2 s at 0g), and again a hyper-gravity period. During the first two days, devoted to the thermal characterization, the device has been heated up at the desired temperature before the micro-gravity occurrence and the power was kept constant throughout each sequence. During the third day, devoted to the startup phenomena, the device has been heated up just after the occurrence of microgravity in order to prove that the incipience of the fluid motion is induced by the thermal effect and not by the inertial effects. To let the PHP equilibrate thermally at T_c, the power has not been switched during some parabolas. We discuss here only the parabolas where the initial temperature was homogeneous enough and the plug flow was detectable in the transparent section. The flow and the temperature distribution in the transparent section have been detected by the analysis of the images obtained with the a long wave infrared (IR) camera (AIM®, bandwidth 3 – 5 μm, 1280 × 1024 pixels, resolution 40 μm). The method of analysis of the IR images is described by Catarsi *et al.* [3].

2.1. CASCO Simulations

The CASCO approach is 1D. The code is stable and computationally efficient: the simulation described below takes several minutes at the desktop PC. The specific PHP parameters used for the simulation are listed in the Table below. The PHP geometry (location and size of the evaporator, condenser and adiabatic sections, turn number, etc.) is that of Fig. 1. The structure

of the PHP is specific, with three adiabatic sections per PHP turn as measured along the tube: between the evaporator and the 1st condenser, between two condensers, and between the 2nd condenser and the evaporator section of the next turn. Since the thermal gradients are measured to be extremely low in the spreader, it is assumed isothermal so its temperature T_e depends only on time. It is found from the energy balance of the spreader

$$C_s \frac{\mathrm{d}T_e}{\mathrm{d}t} = P_e - \pi d_e \int q_s(x)\mathrm{d}x; \qquad q_s(x) = U_s[T_e - T_w(x)] \tag{1}$$

where $C_s = \rho_s V_s c_s$ is its equivalent thermal mass; ρ_s is its density; V_s is its volume; c_s is its heat capacity; P_e is the input power; d_e is the external tube diameter; q_s is the heat flux from the spreader to the tube; T_w is the temperature of the internal tube wall. Integration is performed over 14 evaporator sections of the tube. To adequately describe the empty PHP dynamics, it was necessary to introduce the contact thermal resistance between evaporator spreader and the tubes. The corresponding contact thermal conductance U_s have been adjusted (together with C_s) by using the experimental data on the empty PHP. T_w is determined from the equation

$$\frac{\partial T_w}{\partial t} = D_w \frac{\partial^2 T_w}{\partial x^2} + \frac{j_w}{\rho_w c_w}; \qquad j_w = \frac{\pi}{S_w} \begin{cases} d_e\, q_s - d\, q_{fluid} & \text{if } x \in \text{evaporator} \\ -d\, q_{fluid} & \text{if } x \in \text{adiab. sec.} \end{cases} \tag{2}$$

where ρ_w is the tube density; c_w is the tube heat capacity; $S_w = 0.25\pi(d_e^2 - d^2)$ is its cross-section; d is the inner tube diameter; q_{fluid} is the wall to fluid heat flux defined in [4]. Note that the constant temperature $T_w = T_c$ is imposed within the condenser sections. The same set of parameters was used for all the simulations.

Evaporator length	12 mm
Lengths of condenser sections	80 mm, 80 mm
Length of adiabatic section	32 mm, 10 mm, 218 mm
Number of turns, Nturn	14
Length of the feed-back section	84 mm
Turn curvature radius	8 mm
Outer tube diameter, de	5 mm
Inner tube diameter, d	3 mm
Time step	0.1 ms
Tube mesh spacing	2 mm
Liquid mesh spacing (approximately)	1 mm
Parameters obtained by fitting to the experimental data	
Thermal mass of evaporator spreader, Cs	67 J/K
Contact thermal conductance, Us	1600 W/(m2K)
Liquid film thickness	72 μm
Vapor bubble nucleation barrier	5 K

Unfortunately, the 20 s micro-gravity duration is too small to achieve a stable functioning regime so the transient simulation is required. The data are then dependent on the initial phase distribution, which is however unknown because the most of PHP is opaque. One can only reasonably guess that (i) the liquid gathers at the evaporator side due to the vertical favorable orientation of PHP during the hyper-gravity period preceding micro-gravity and (ii) a continuous liquid film is deposited over the internal tube walls during preceding parabolas.

3. Results and discussion

Comparisons of the temperatures measured experimentally and simulated with CASCO are presented in Figs. 2 - 8. The temperatures of the evaporator spreader T_e, and tube wall temperatures in adiabatic section close to evaporator (TC5, TC7, TC10) and condenser (TC6, TC9, cf. Fig. 1) are compared. The agreement is very good. The velocities of liquid plugs (Figs. 9 and 10) are also quite similar. In the case of Fig. 9, the simulation captures closely the evolution for t <5 s. For t >5 s, the velocity modulus is reproduced, but not the sign. The reason is the unknown initial phase distribution inside the tube. Similar results are obtained for the case in Fig. 10. In Figs. 11 and 12, a comparison of liquid plug lengths in shown. The different plugs visible in the transparent section during the start-up are shown with different colors; in both cases there is a qualitative agreement. Finally, Figs. 13 and 14 show the experimental and simulated temperature distribution along the liquid plugs, respectively; one can see the sharp temperature variation near the menisci both in the experimental and simulation data. For the first time in the literature, at least to the authors' knowledge, a multi-parametric transient comparison has been done quantitatively on several physical variables such as fluid and wall temperatures and plug lengths and velocities. The agreement of the experimental and simulation data is satisfactory, which shows a validity of CASCO.

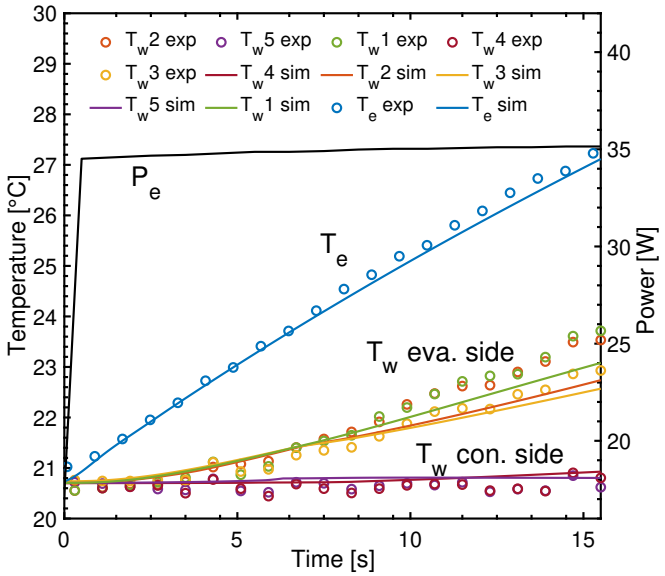

Figure 2. Evolution of the temperatures and $P_e \simeq 35$ W during parabola 2.

Acknowledgments

The present work is supported by the project TOPDESS, financed through the Microgravity Application Program by the European Space Agency. An additional financial support of CNES awarded to VN through GdR MFA is acknowledged.

References

[1] Gu J, Kawaji M and Futamata R 2005 *Microgravity Sci. Technol.* **16** 181
[2] Daimaru T, Yoshida S and Nagai H 2017 *Appl. Therm. Eng.* **113** 1219
[3] Catarsi A, Fioriti A, Mameli M, Filippeschi S and Di Marco P 2018 *Proc. 16th Int. Heat Transf. Conf.* (Beijing, China)
[4] Nikolayev VS 2011 *J. Heat Transfer* **133** 081504
[5] Nekrashevych I and Nikolayev VS 2017 *Appl. Therm. Eng.* **117** 24
[6] Nikolayev VS 2021 *Appl. Therm. Eng.* **195** 117111

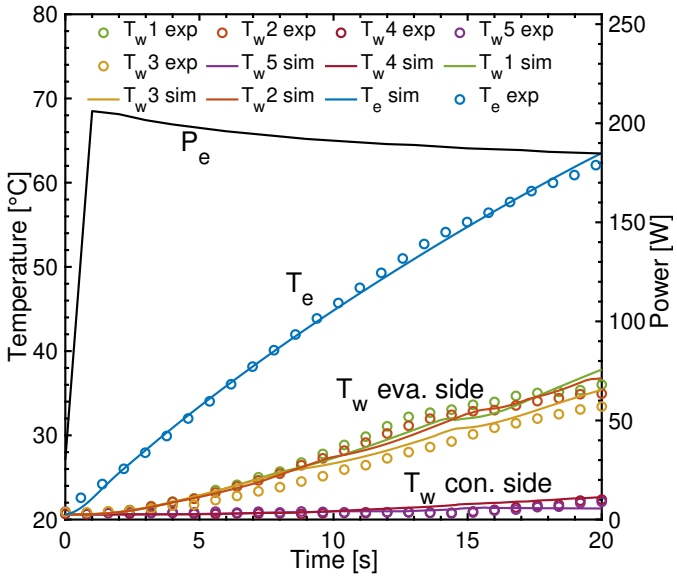

Figure 3. Evolution of the temperatures and $P_e \simeq 205$ W during parabola 19.

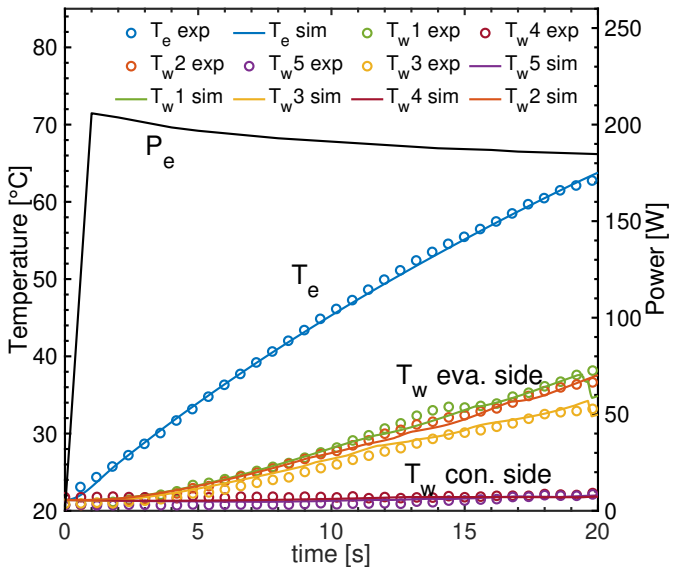

Figure 4. Evolution of the temperatures and $P_e \simeq 200$ W during parabola 16.

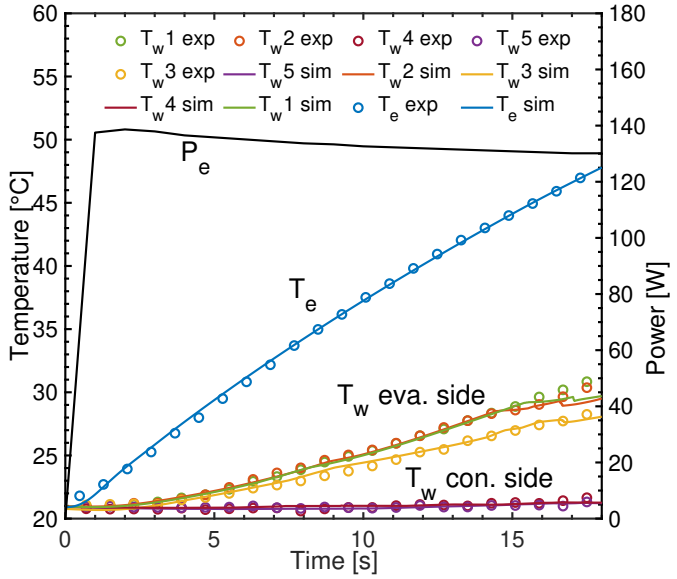

Figure 5. Evolution of the temperatures and $P_e \simeq 135$ W during parabola 22.

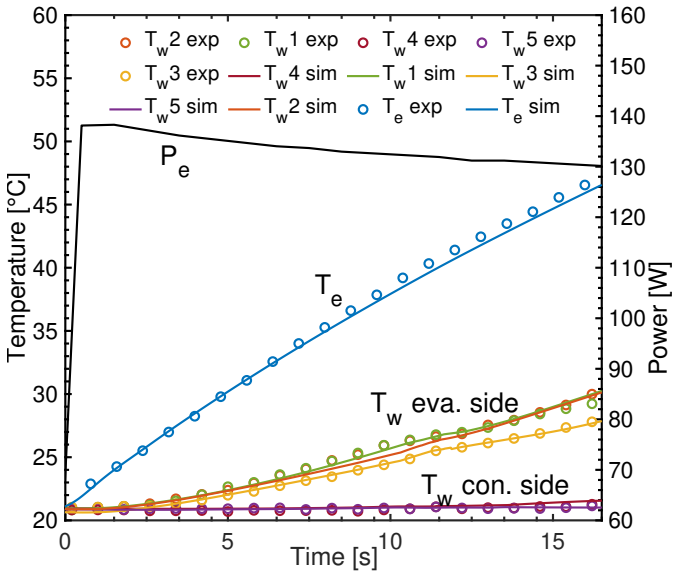

Figure 6. Evolution of the temperatures and $P_e \simeq 135$ W during parabola 25.

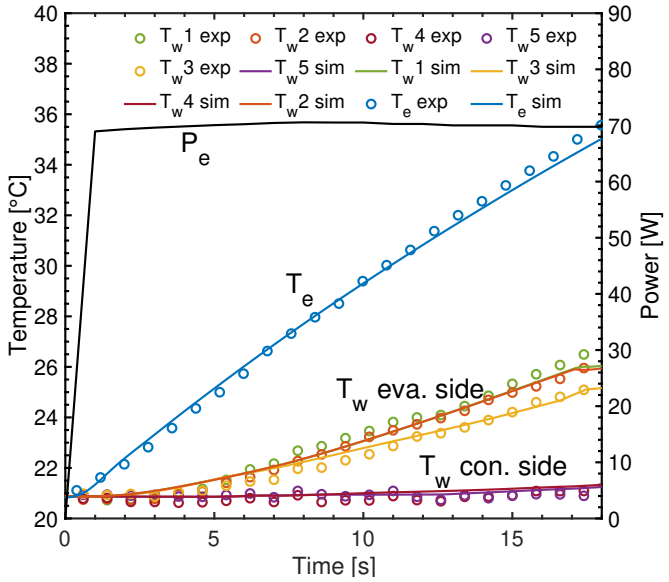

Figure 7. Evolution of the temperatures and $P_e \simeq 70$ W during parabola 27.

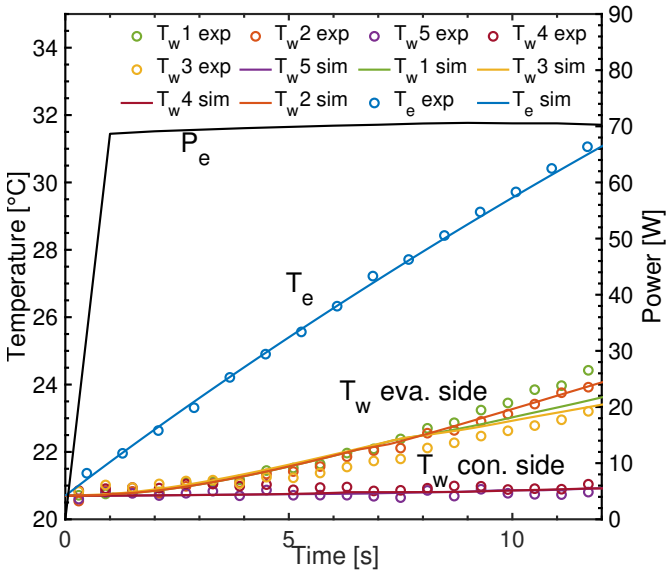

Figure 8. Evolution of the temperatures and $P_e \simeq 70$ W during parabola 30.

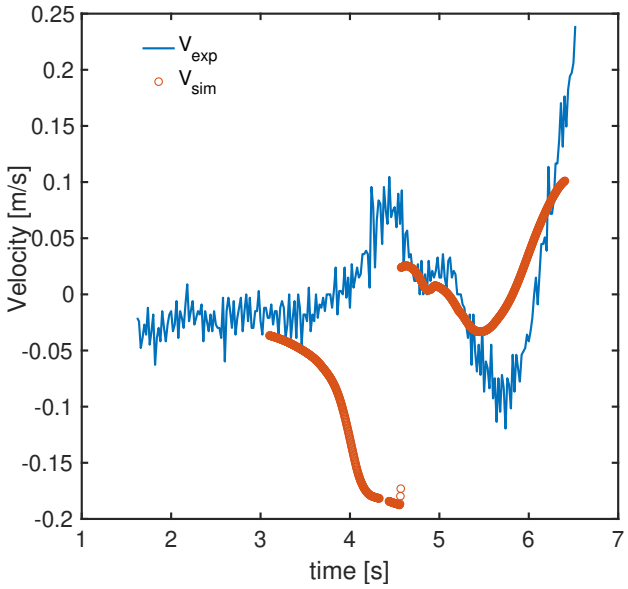

Figure 9. Temporal evolution of liquid plug velocities during parabola 19. Experimental velocity is in blue; simulated, in orange.

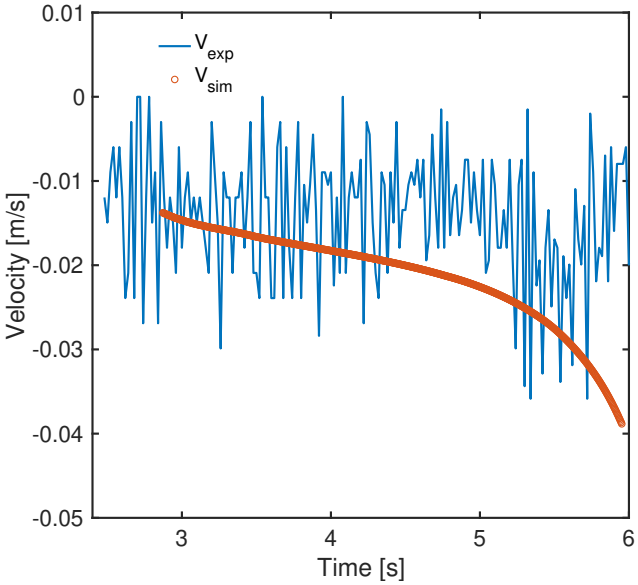

Figure 10. Temporal evolution of liquid plug velocities during parabola 30. Experimental velocity is in blue; simulated, in orange.

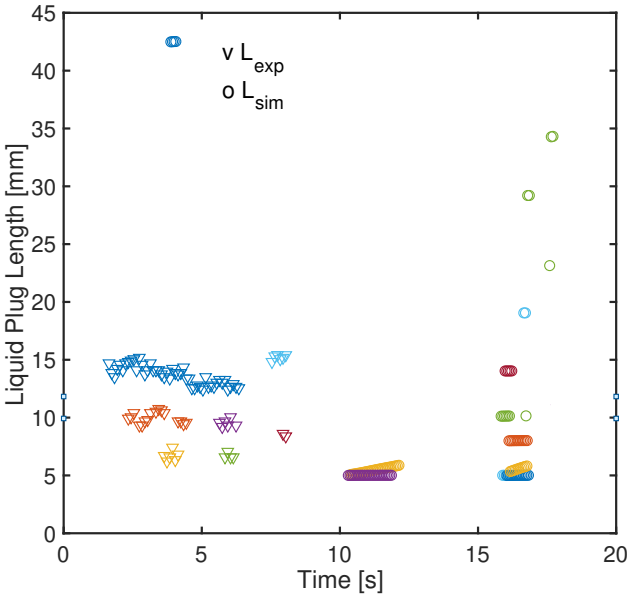

Figure 11. Evolution of liquid plug lengths during parabola 19. Experimental lengths are shown with crosses; simulated, with circles.

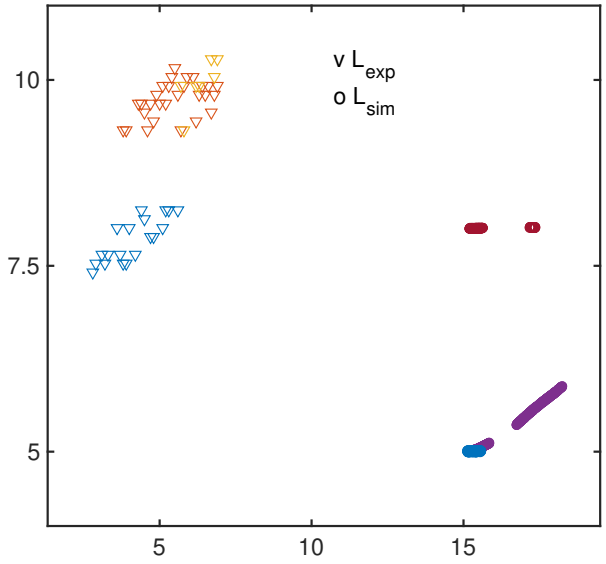

Figure 12. Evolution of liquid plug lengths during parabola 30. Experimental lengths are shown with crosses; simulated, with circles.

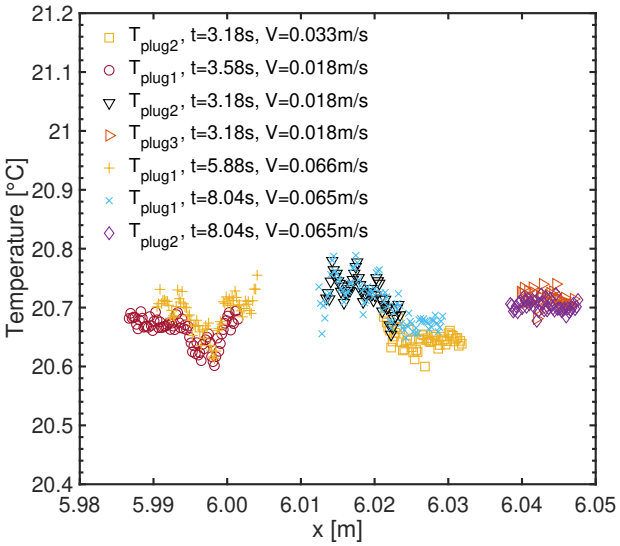

Figure 13. Experimental temperature distribution along liquid plugs during parabola 19.

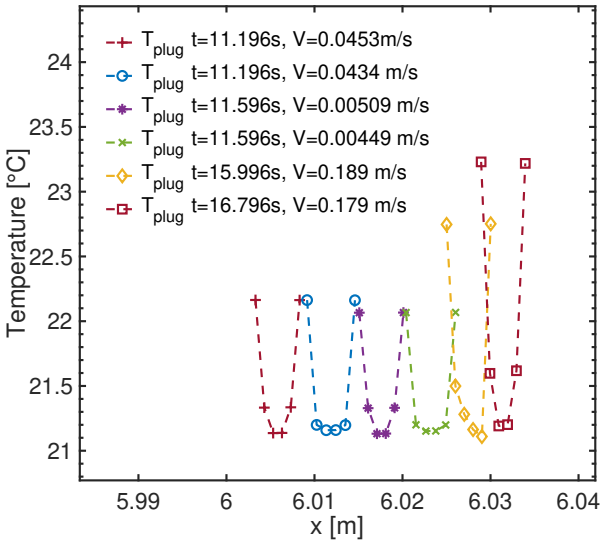

Figure 14. Simulated temperature distribution along liquid plugs during parabola 19.